specific region is a critical element of the electrodynamic problem and that its influence should be interpreted within the constraints of thermodynamic equilibrium between the two components of a dielectric junction. This equilibrium constraint can be understood as a phase equilibrium at the junction that even at monolayer levels requires an interface phase; this interface phase controls the overall junction electrostatics via a Coulomb buffer. This Coulomb buffer is fundamentally distinct from the wave function decay of interface states that comes from the classical bulk-termination view of the barrier-height problem. Moreover, this thermodynamic-electrodynamic view of the problem provides a unifying concept for understanding and designing barrier-height functions within the barrier-offset problem that is general to all of semiconductor physics.

References and Notes

1. W. Schottky, *Phys. Z.* **113**, 367 (1940).
2. N. F. Mott, *Proc. Cambridge Philos. Soc.* **34**, 568 (1938).
3. R. L. Anderson, *Solid-State Electron.* **5**, 341 (1962).
4. For a review of these issues, see the monograph by W. Monch, *Semiconductor Surfaces and Interfaces* (Springer, Berlin, ed. 3, 2001).
5. A. Franciosi, C. G. Van de Walle, *Surf. Sci. Rep.* **25**, 1 (1996).
6. A. A. Demkov, O. F. Sankey, *Phys. Rev. Lett.* **83**, 2038 (1999).
7. S. G. Louie, M. L. Cohen, *Phys. Rev. B* **13**, 2461 (1976).
8. W. R. Frensley, H. Kroemer, *Phys. Rev. B* **16**, 2642 (1977).
9. W. A. Harrison, E. A. Kraut, J. R. Waldrop, R. W. Grant, *Phys. Rev. B* **18**, 4402 (1978).
10. J. Tersoff, *Phys. Rev. Lett.* **52**, 465 (1984).
11. W. A. Harrison, J. Tersoff, *J. Vac. Sci. Technol. B* **4**, 1068 (1986).
12. W. Monch, *Appl. Phys. Lett.* **72**, 1899 (1998).
13. A. Baldereschi, S. Baroni, R. Resta, *Phys. Rev. Lett.* **61**, 734 (1988).
14. M. Peressi, S. Baroni, R. Resta, A. Baldereschi, *Phys. Rev. B* **43**, 7347 (1991).
15. F. Leonard, J. Tersoff, *Phys. Rev. Lett.* **84**, 4693 (2000).
16. R. T. Tung, *Phys. Rev. Lett.* **84**, 6078 (2000).
17. R. T. Tung, *Phys. Rev. B* **64**, 205310 (2001).
18. R. T. Tung, *Mater. Sci. Eng.* **35**, 1 (2001).
19. J. Robertson, *J. Vac. Sci. Technol. B* **18**, 1785 (2000).
20. P. Ghosez, K. M. Rabe, *Appl. Phys. Lett.* **76**, 2767 (2000).
21. R. A. McKee, F. J. Walker, M. F. Chisholm, *Science* **293**, 468 (2001).
22. R. A. McKee, F. J. Walker, M. F. Chisholm, *Phys. Rev. Lett.* **81**, 3014 (1998).
23. R. A. McKee, F. J. Walker, J. R. Conner, R. Raj, *Appl. Phys. Lett.* **63**, 2818 (1993).
24. R. A. McKee, F. J. Walker, E. D. Specht, G. E. Jellisen, L. A. Boatner, *Phys. Rev. Lett.* **72**, 2741 (1994).
25. A. P. Sutton, R. W. Balluffi, in *Interfaces in Crystalline Materials* (Clarendon Press, Oxford, 1995), pp. 349–394.
26. E. A. Kraut, R. W. Grant, J. R. Waldrop, S. P. Kowalczyk, *Phys. Rev. Lett.* **44**, 1623 (1980).
27. Materials and methods are available as supporting material on *Science* Online.
28. Calculations in this work have been done with the use of the PWscf package (S. Baroni, A. Dal Corso, S. de Gironcoli, P. Giannozzi, Plane Wave Self-Consistent Field, Trieste, Italy), available online at www.pwscf.org/.
29. A. M. Stoneham, J. Dhote, "A compilation of crystal data for halides and oxides" (University College London, London, 2002), available online from www.cmmp.ucl.ac.uk/~ahh/research/crystal/homepage.htm, and references contained therein.
30. We acknowledge the careful review and comments on our manuscript provided by G. Ice, M. Chisholm, D. Nicholson, L. Christiaens, and C. McKee. Research sponsored jointly by the Defense Advanced Research Projects Agency (DAAS19-01010-650) and the Division of Materials Sciences and Engineering, Office of Basic Energy Sciences, U.S. Department of Energy at Oak Ridge National Laboratory under contract DE-AC05-00OR22725 with UT-Battelle, Limited Liability Corporation, and at the University of Tennessee under contract DE-FG02-01ER45937.

Interference of Quantized Transition-State Pathways in the H + D₂ → D + HD Chemical Reaction

Dongxu Dai,[1] Chia C. Wang,[2,3] Steven A. Harich,[1,2] Xiuyan Wang,[1] Xueming Yang,[1,2,4]* Sheng Der Chao,[5] Rex T. Skodje[5]*

The collision-energy dependence of the state-resolved differential cross section at a specific backward-scattering angle for the reaction H + D₂ → D + HD is measured with the D-atom Rydberg "tagging" time-of-flight technique. The reaction was modeled theoretically with converged quantum scattering calculations that provided physical interpretation of the observations. Oscillations in the differential cross sections in the backward-scattering direction are clearly observed and are attributed to the transition-state structures that originate from the interferences of different quantized transition-state pathways.

During a reactive molecular collision, the transition state (TS) acts as a bottleneck so that incident reagent flux below the TS energy is reflected, whereas above the TS energy it is transmitted to products. Taken literally, transition-state theory is based on the existence of rotational-vibrational (ro-vib) quantum states of the collision complex lying near the maxima of effective potential barriers (1). These quantized bottleneck states (QBSs) are labeled by the quantum numbers for motion orthogonal to the reaction coordinate; in the case of a three-atom reaction with a collinear reaction path, we can use the designation $(v_{sym-str}, v_{bend}^{\Lambda})$. Suitably averaged measures of reaction rate, such as the cumulative reaction probability, $N_R(E)$ (the sum of the reaction probability over all open initial and final states at a fixed energy and angular momentum, E and J), are theoretically found to exhibit a staircase structure versus E as the QBS energies are passed (1).

Despite the crucial importance of the QBSs to the framework of chemical reaction dynamics, they have proven quite elusive to direct experimental observation. The work of Moore and co-workers (2) on the laser photolysis of the ketene molecule in a cold jet environment revealed steplike structures in the rate for $C_2H_2O + h\nu \rightarrow CO + CH_2$ as the deposited energy passed through threshold values (where $h\nu$ is photolysis energy). However, the conjecture that the steps were associated with the energies of the QBS was cast into doubt by strong disagreement with theoretical results (3). In a full-collision experiment, appropriate to bimolecular reactions, direct observation of quantum states in the TS region is even more difficult. The core problem is that the impact parameter averaging in a crossed-beam scattering experiment smears the bottleneck energies over a large range. Many state- and angle-resolved studies (4) have focused on the F + H₂ and H + H₂ reactions, and their isotopic variants, as a function of collision energy, E_C. In the former reaction, quantum effects arise as the result of a Feshbach resonance that causes a resonance step to appear in the integral cross section (ICS) (5) and forward peaks in certain state-to-state differential cross sections (DCSs) (6). In the H + D₂ reaction, forward scattering of products has been observed (7) and attributed to a time-delay mechanism (8). The forward-scattering peak was attributed to a QBS by Truhlar and co-workers (9). In a

¹State Key Laboratory of Molecular Reaction Dynamics, Dalian Institute of Chemical Physics, Chinese Academy of Sciences, Dalian, China. ²Institute of Atomic and Molecular Sciences, Academia Sinica, Post Office Box 23166, Taipei, Taiwan. ³Department of Chemistry, National Taiwan University, Taipei, Taiwan. ⁴Department of Chemistry, National Tsing Hua University, Hsinchu, Taiwan. ⁵Department of Chemistry and Biochemistry, University of Colorado, Boulder, CO 80309, USA.

*To whom correspondence should be addressed. E-mail: xmyang@po.iams.sinica.edu.tw (X.Y.), skodje@spot.colorado.edu (R.T.S.)

previous study (*10*, *11*), we found evidence for QBSs in the H + HD reaction through a mechanism whereby the slowing of motion near the TS gave rise to a forward peak in the DCS at fixed E_C that is unrelated to Feshbach resonances.

Despite these detailed measurements, it is still not obvious a priori how the QBS should show up in the observations versus E_C, because the staircase function is appropriate for $N_R(E)$ but not for state-to-state cross sections. We present here the results of a further study of the H + D₂ → D + HD reaction (*12–16*) that demonstrate the influence of QBSs in a full-collision environment, and the results of a theoretical analysis that provide a physical picture of the underlying dynamics involving the QBS.

To observe the effects of quantized transition states in a reactive collision, it is essential to accurately measure the reactive cross sections as a function of variable E_C. In a previous experiment on the H + HD → D + H₂ reaction (*10*, *11*), we measured the state-to-state DCS at two isolated collision energies with a crossed molecular beam apparatus using a HI-photolysis source for the H-atom beam at fixed laser frequencies. In the present experiment on the related H + D₂ → D + HD reaction, we modified our previous experimental design to permit the use of a tunable photolysis laser to generate the H-atom beam with variable speed, which thus allows the continuous variation of E_C.
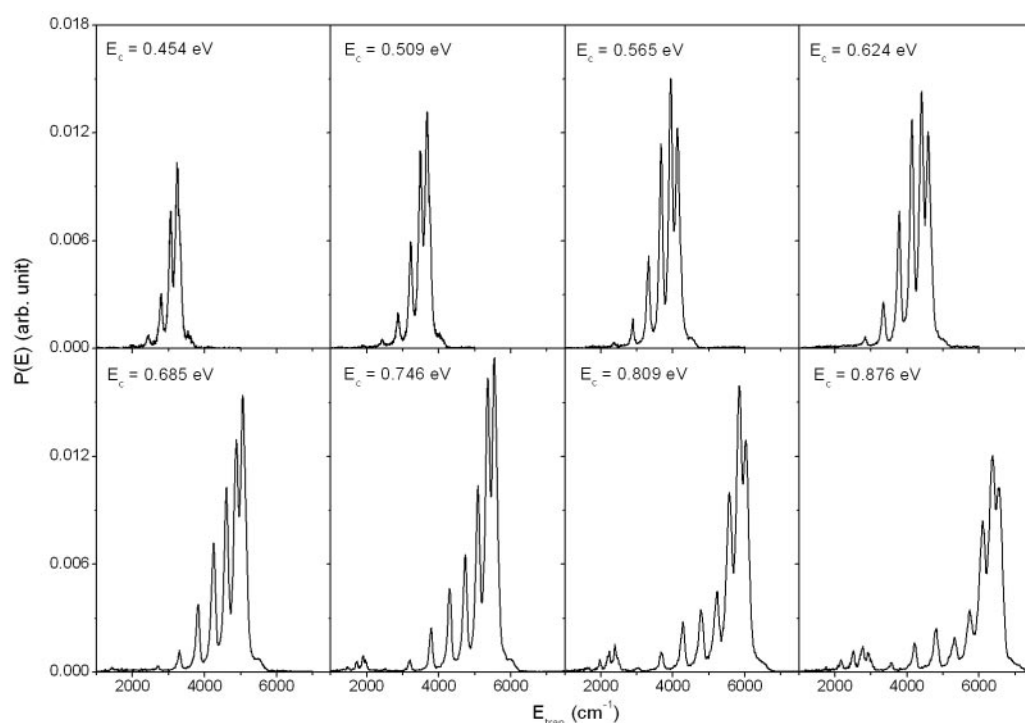
Except for the photolysis source, the present experiment is similar in design to our previous work (*10*, *11*). Two parallel molecular beams (HI and ortho-D₂) are generated with pulsed

valves. The ortho-D₂ beam was produced by an adiabatic expansion through a nozzle cooled to the liquid nitrogen temperature, which ensures that almost all molecules in the beam are in the $D_2(v = 0, j = 0)$ state (*17*). The H-atom beam is produced by HI-photolysis with a tunable, narrow-band doubled dye laser output. Varying the laser frequency yielded center-of-mass (CM) collision energies in the range $E_C = 0.4$ to 1.0 eV with a spread estimated to be about $\Delta E_C = 10$ meV. The reaction products were monitored with the highly sensitive hydrogen Rydberg atom time-of-flight (TOF) technique originally developed by Welge and co-workers (*17*, *18*). The TOF spectra of D atoms at different E_C values were measured with this method and then converted to the CM translational-energy distribution. Sharp structures are observed in the TOF spectra at different E_C values, which can be assigned to HD-product ro-vib states, which then yield relative quantum state–specific DCSs. Experimental error bars on the DCSs are about ±10% or less. DCSs have been measured previously for the title reaction at individual collisional energies (*8*, *17*, *18*), but the DCSs measured at different collision energies in these previous works have not been calibrated on the same scale. To measure the collision energy–dependent DCS for each product quantum state quantitatively, one has to monitor the beam intensities, especially the H-atom beam intensity, which varies at different collision energies, to provide an accurate calibration for the DCS at different collision energies. The present experimental design, which

could monitor conveniently the H-atom beam intensity in situ, allows the measurement of the absolute DCS up to a single overall scaling factor for all energies and, thus, all product states. The D-atom TOF spectrum was measured at 19 energies at the same (nearly) backward-scattering direction at the laboratory angle of 70°, corresponding to CM angles around 160° for H + $D_2(v = 0, j = 0)$ → HD($v = 0, j' = 2$) + D. Eight typical translational-energy distributions for various E_C values, obtained from the measured D-atom TOF spectra, are shown in Fig. 1. The measured DCSs at laboratory angle $\Theta_L = 70°$ for the HD($v = 0, j' = 2$) products, which were clearly resolved in the TOF spectra, are shown in Fig. 2. Three oscillations in the measured DCS are apparent over the energy range considered. Similar oscillations are also observed for other final states. The observation of this oscillation is intriguing, because the nature of such structures has not been clearly characterized theoretically.

The reaction dynamics for H + D₂ → D + HD was theoretically modeled with a fully converged coupled-channel scattering calculation that used the highly accurate BKMP2 potential energy surface (*19*). These computations produce the S-matrix from a coupled-channel calculation in a hyperspherical coordinate system (*20–23*) based on a partial wave expansion up to total angular momentum $J = 32$ on a grid of 90 total energies (including zero-point) from $E = 0.5$ to 1.6 eV. The details of the calculations have been presented elsewhere (*16*), and it is sufficient to note that the state-to-state DCS

Fig. 1. Typical translational energy distributions for H + D₂($v = 0, j = 0$) → D + HD(v', $j' = 2$), which were obtained from the measured D-atom TOF spectra at eight different collision energies.

Fig. 2. The experimental differential cross section (dots) for H + D$_2$($v = 0$, $j = 0$) → D + HD($v' = 0$, $j' = 2$), measured at the laboratory angle of 70°, versus the CM collision energy, E_C. The curve is the result of the quantum scattering calculation. The transformation from LAB to CM is energy dependent.

HD(v=0,j'=2) at Θ_{LAB} = 70°
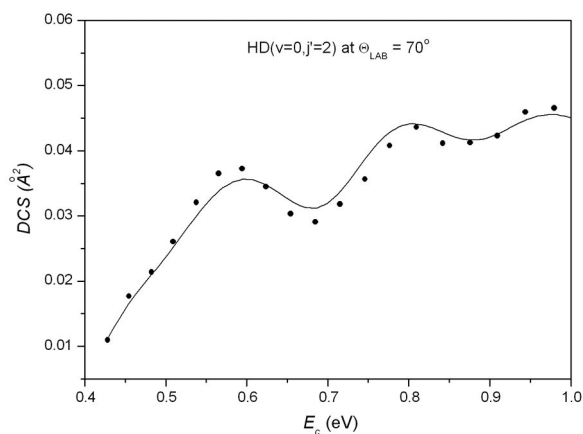
and ICS are converged with respect to basis set size and propagation steps. The experimental DCS at $\Theta_L = 70°$ ($\Theta_{CM} \approx 160°$) for H + D$_2$(0,0) → HD(0,2) + D is well reproduced by theory (Fig. 2).

We can now trace the physical origin of the intriguing oscillatory structure of the DCS. One notable feature that emerges from the scattering calculations is the occurrence of very strong oscillations in the S-matrix elements versus E, and thus also in the state-to-state reaction probabilities obtained from helicity averaging, $P_R(v, j \rightarrow v', j';E)$. They are apparent in most scattering channels and for broad ranges of the total angular momentum, J, that labels the partial wave. Figure 3B shows the oscillation for the product HD(0,2) for the case $J = 0$. A similar oscillation in $P_R(v, j \rightarrow v', j';E)$ has been computed for other isotopic combinations of this reaction (24), but it is most pronounced in the present case. The oscillatory structure taken as a function of J reveals that the peak positions progressively shift to higher energy with increasing J. This "J-shifting" of features in P_R versus J is a well-known manifestation of impact parameter averaging and leads to the energy smearing of features, such as resonance energies, in collision experiments. Indeed, when the partial waves are combined to form the cross sections, $\sigma_R(v, j \rightarrow v', j';E) \sim E_c^{-1}\Sigma_J(2J + 1)P_R(v, j \rightarrow v', j';E, J)$, the oscillations are generally averaged out. Faint traces of the oscillations do survive in the ICS for certain final states (16), although these weak residuals are probably below the present experimental detection limit. The situation is clearly different for the DCS. As shown in Fig. 2, the oscillatory structures in the backward (i.e., rebound) direction appear much more strongly than the corresponding structures in the ICS. Angle selection suppresses the impact parameter averaging and allows the strong oscillation of the individual S-matrix elements to persist in the final observable oscillations. Quantitative analyses in this work show that the backward scattering is dominantly the result of low-impact-

parameter scattering and is dominated by the contributions of small J, i.e., $J < 15$. In this way, the structure apparent in $P_R(v, j \rightarrow v', j';E)$ survives more robustly in the DCS than in the ICS and is thus more amenable to direct observation. Therefore, detecting backward-scattering products at low rotational excitation is selectively probing reactive products from collisions with a reduced range of small impact parameters.

The oscillation in the DCS is the result of an underlying oscillation in P_R, but why does P_R oscillate in the first place? In previous discussions of the H + H$_2$ reaction family, there is occasional reference to such structures as resonance peaks (25), although a systematic assignment has not appeared. However, it does not appear that this simple identification is tenable. Using the spectral quantization method (26, 27), we computed all the localized quantum states for $E_C < 1.2$ eV and found that all the relevant lowest energy states can be assigned to the QBSs $E_C(0,0^0) = 0.41$ eV, $E_C(0,2^0) = 0.59$ eV, and $E_C(1,0^0) = 0.71$ eV, all for $J = 0$. Although the QBSs are sometimes referred to as "barrier resonances," this nomenclature is controversial precisely because P_R does not show resonant peaks. Moreover, the peak positions (16) are out of phase for the various transitions ($v, j \rightarrow v', j'$) (Fig. 3B), whereas resonance peaks should appear at nearly the resonance energy. Finally, the amount of J-shifting of the peaks is inconsistent (16) with a progression of rotationally excited resonance states. Even though the oscillations are not resonance peaks per se, they are intimately connected to the QBSs. As expected, the computed $N_R(E)$ displayed in Fig. 3A shows a series of steps roughly modeled by the classical staircase function

$$S(E) = \sum_n \theta(E - \varepsilon_n),$$

where ε_n are the QBS energies and θ is the Heaviside step function. The out-of-phase oscillations of the individual $P_R(v, j \rightarrow v', j';E)$ hence combine to yield the steps in $N_R(E)$.

Instead, it appears that the energy-dependent oscillation of the state-to-state reaction probabilities, and hence of the backward
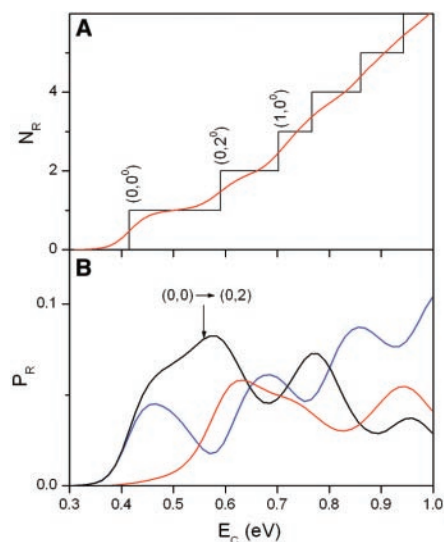

Fig. 3. (**A**) The solid line is the cumulative reaction probability, $N_R(E)$, versus E_C for $J = 0$. The staircase function $S_R(E)$ is computed with Heaviside step functions at the bottleneck energies. (**B**) The $J = 0$ reaction probability $P_R(v = 0, j = 0 \rightarrow v', j';E)$ versus E_C for the cases (v', j') = (0,0) (blue), (0,2) (black), and (0,6) (red). The reactive steps observed in $N_R(E)$ are built up from the sum of the out-of-phase oscillations in P_R.

DCS, is an interference effect somewhat similar to Stuckelberg oscillations (28) familiar from atomic physics. The correlation diagram shown in Fig. 4A provides a simple view of the reaction dynamics. The QBSs near the saddle point are correlated along the reaction coordinate, s, to the asymptotic ro-vib states through vibrationally adiabatic potential curves. Coupling between the curves occurs in the entrance and exit channels as a result of effects such as avoided crossings. Near the saddle point, where the levels are farther apart, the dynamics is more uncoupled. The reactive steps in N_R are manifestations of the uncoupled dynamics near the TS, because the channel interactions are largely averaged out. However, this averaging does not occur in $P_R(v, j \rightarrow v', j';E)$. The incident flux in a particular reagent channel, H + D$_2$(v, j), is redistributed among several neighboring states because of vibrationally nonadiabatic coupling in the entrance channel (Fig. 4A). Thus, several QBS thresholds control the reactive flux as it passes the TS. Similar coupling again scrambles the flux in the exit channel of the reaction. Hence, one expects that each state-to-state reaction probability is affected by a number of QBS pathways and is formed from the coherent sum of amplitudes corresponding to a variety of pathways, as depicted schematically in Fig. 4A.

On the basis of this physical view of the reaction dynamics, a very broad class of models can be constructed that yield qualitatively similar oscillations of the reaction probabilities. We can write the total S-matrix as $\mathbf{S}(E) = \mathbf{S}_0^- \cdot \mathbf{S}_{na}^- \cdot \mathbf{S}_b \cdot \mathbf{S}_{na}^+ \cdot \mathbf{S}_0^+$. Here, $\mathbf{S}_0^\pm$

Fig. 4. (**A**) A schematic correlation diagram illustrating the role of QBS on the reaction dynamics. Because of nonadiabatic coupling in the entrance channel, flux in a given initial state will pass the transition state through several bottleneck states. Nonadiabatic coupling in the exit channel will further mix the reactive flux into the final product states. A simple model of the form $S(E) = S_0^- \cdot S_{na}^- \cdot S_b \cdot S_{na}^+ \cdot S_0^+$ is used for predicting. The barrier component, S_b, is represented by a set of Eckart barriers with heights equal to the QBSs. The constant nonadiabatic couplings, $S_{na}^\pm$, couple most strongly the states with $j = j'$, $j' \pm 1$, and $j' \pm 2$. (**B**) The state-to-state reaction probabilities, $P_R(0,0 \rightarrow 0, j';E)$ versus E_C for $j' = 0$ (black), 1 (red), 2 (blue) predicted by the simple model shown in (A). The solid lines show that the full model,
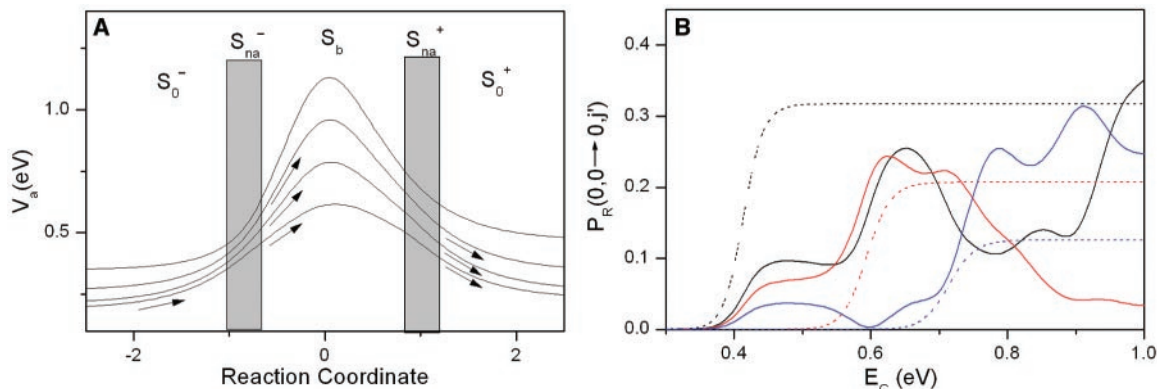
with coupling in both the entrance and exit channels, exhibits the out-of-phase oscillations observed in the exact reaction dynamics. The dashed lines show the results when the coupling in the exit channel is switched off, which then shows only simple threshold behavior. The essential point is that all physically reasonable models of this form show oscillations qualitatively similar to those observed in the exact calculation.

Fig. 5. The probabilities density for the $J = 0$ scattering wave function, $\Psi_E(R)$, sliced along the perpendicular to the minimum energy path at the saddle point, plotted in the bending (vertical direction) and symmetric stretch (horizontal direction) normal coordinates. Three density plots are shown in this figure at three different collision energies: 0.40, 0.70, and 0.95 eV. These three collision energies are slightly above the three different QBSs: $(0,0^0)$, $(0,2^0)$, and $(1,0^0)$ at the saddle point, correspondingly. The plots illustrate the sequential contribution of the different QBSs with increasing collision energy.
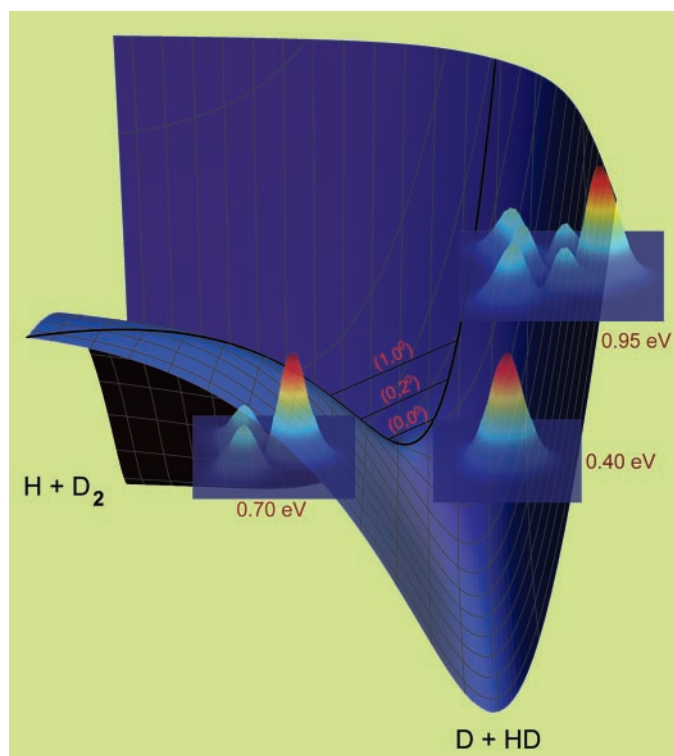
tum dynamics, we have computed the full scattering wave function, $\Psi_E(R)$, as a function of E_C for H + D_2(0,0) for $J = 0$ by Fourier filtering a time-dependent quantum wave packet. To visualize the dynamics near the transition state, we make a two-dimensional slice of $\Psi_E(R)$ orthogonal to the reaction path at the saddle point and watch the state evolution as E_C is changed. The probability densities obtained are plotted in the symmetric stretch and bending coordinates (Fig. 5). At low energy, $E_C = 0.4$ eV, which is near the threshold of the DCS, the wave function is nodeless and reflects barrier passage only through the lowest QBS, $(0,0^0)$. At the position of the second peak of the DCS, $E_C = 0.7$ eV, we clearly see the contribution from the next QBS, which is the bend excited state $(0,2^0)$. Finally, near the third peak energy at $E_C = 0.95$ eV, we see next that QBS has grown in proportion to the symmetric stretch excited state $(1,0^0)$. Obviously, the wave function will become quite complicated at high energies because of the coherent sum of many bottleneck states, but the assignment of the first three contributions is quite clear.

and $S_{na}^\pm$ represent the free asymptotic and the curve-hopping dynamics, respectively, in the entrance and exit channels, whereas S_b is the uncoupled propagation along a series of barriers near the transition state. Near a QBS energy (i.e., a barrier maximum), a new term in S_b will switch on. The effect of this threshold behavior in the full $S(E)$ is then redistributed among the channels through $S_{na}^\pm$. The appearance of a peak or a valley in P_R is determined by the interference with the other components of the flux. A model based on Eckart barriers and constant nonadiabatic coupling to mimic H + D_2 yields out-of-phase oscillations in

$P_R(0,0 \rightarrow 0, j';E)$ analogous to those observed in the full quantum scattering calculation (Fig. 4B). Note, however, that if the recoupling in the exit channel is omitted (as shown in Fig. 4B with dashed lines), then oscillations disappear and P_R exhibits simple steps at the QBS energies. Because the occurrence of the oscillation is quite insensitive to the details of the model, the interference of pathways through the network of QBS seems to provide a robust mechanism for the oscillating reaction probabilities.

Finally, to directly observe the influence of the QBSs on the exact three-dimensional quan-

References and Notes

1. D. C. Chatfield, S. L. Mielke, T. C. Allison, D. G. Truhlar, *J. Chem. Phys.* **112**, 8387 (2000).
2. S. K. Kim, E. R. Lovejoy, C. B. Moore, *J. Chem. Phys.* **102**, 3202 (1995).
3. J. D. Gezelter, W. H. Miller, *J. Chem. Phys.* **104**, 3546 (1996).
4. K. Liu, *Annu. Rev. Phys. Chem.* **52**, 139 (2001).
5. R. T. Skodje et al., *Phys. Rev. Lett.* **85**, 1206 (2000).
6. D. M. Neumark et al., *Phys. Rev. Lett.* **53**, 226 (1984).
7. F. Fernandes-Alonso et al., *Angew. Chem. Int. Ed. Engl.* **39**, 2748 (2001).
8. S. C. Althorpe et al., *Nature* **416**, 67 (2002).
9. T. C. Allison, R. S. Friedman, D. J. Kaufman, D. G. Truhlar, *Chem. Phys. Lett.* **327**, 439 (2000).
10. S. A. Harich et al., *Nature* **419**, 281 (2002).
11. S. A. Harich et al., *J. Chem. Phys.* **117**, 8341 (2002).
12. T. N. Kitsopoulos et al., *Science* **260**, 1605 (1993).

13. M. J. D'Mello, D. E. Manolopoulos, R. E. Wyatt, *J. Chem. Phys.* **94,** 5985 (1991).
14. Y. S. M. Wu, A. Kuppermann, *Chem. Phys. Lett.* **235,** 105 (1995).
15. B. K. Kendrick, *J. Chem. Phys.* **114,** 8796 (2001).
16. S. D. Chao, R. T. Skodje, *Chem. Phys. Lett.* **336,** 364 (2001).
17. L. Schnieder, K. Seekamp-Rahn, E. Wrede, K. H. Welge, *J. Chem. Phys.* **107,** 6175 (1997).
18. L. Schnieder *et al.*, *Science* **260,** 1605 (1995).
19. A. I. Boothroyd, W. J. Keogh, P. G. Martin, M. R. Peterson, *J. Chem. Phys.* **104,** 7139 (1996).
20. R. T. Pack, G. A. Parker, *J. Chem. Phys.* **87,** 3888 (1987).
21. G. C. Schatz, *Chem. Phys. Lett.* **150,** 92 (1988).
22. J. M. Launay, M. Le Dourneuf, *Chem. Phys. Lett.* **163,** 178 (1989).
23. D. M. Skouteris, J. F. Castillo, D. E. Manolopoulos, *Comput. Phys. Commun.* **113,** 128 (2000).
24. W. H. Miller, *Ann. Rev. Phys. Chem.* **41,** 245 (1990).
25. S. Sukiasyan, H.-D. Meyer, *J. Phys. Chem. A* **105,** 2604 (2001).
26. R. Sadeghi, R. T. Skodje, *J. Chem. Phys.* **102,** 193 (1995).
27. R. T. Skodje, R. Sadeghi, H. Koppel, J. L Krause, *J. Chem. Phys.* **101,** 1725 (1994).
28. M. S. Child, *Molecular Collision Theory* (Dover, New York, 1996), pp. 161–174.
29. We are grateful to K. Liu for many useful discussions. This work was supported by the National Science Foundation of the United States and by the National Science Council and the Academia Sinica of Taiwan. X.Y. and D.D. also acknowledge support from a pre-973 grant and the 973 project for reaction dynamics from the Ministry of Science and Technology of China.

Impact Ejecta Layer from the Mid-Devonian: Possible Connection to Global Mass Extinctions

Brooks B. Ellwood,[1] Stephen L. Benoist,[1] Ahmed El Hassani,[2] Christopher Wheeler,[1] Rex E. Crick[3]

We have found evidence for a bolide impacting Earth in the mid-Devonian (~380 million years ago), including high concentrations of shocked quartz, Ni, Cr, As, V, and Co anomalies; a large negative carbon isotope shift (–9 per mil); and microspherules and microcrysts at Jebel Mech Irdane in the Anti Atlas desert near Rissani, Morocco. This impact is important because it is coincident with a major global extinction event (Kacák/*otomari* event), suggesting a possible cause-and-effect relation between the impact and the extinction. The result may represent the extinction of as many as 40% of all living marine animal genera.

Earth has a long history of extraterrestrial impact events, with more than 100 documented impact craters (*1*), but to date only the Chixculub crater at the Cretaceous-Tertiary (K-T) boundary event has had enough evidence to suggest a cause-and-effect relation between the impact and the mass extinctions that occurred at the K-T. Such cause-and-effect relations in older formations are harder to evaluate because of the difficulty of correlating among widely separated sections and of precisely pinpointing stratigraphic levels where distal ejecta markers, usually only present in very thin stratigraphic horizons, exist in outcrop. While studying Devonian rocks in Morocco, we found a distinctive magnetic susceptibility pattern (*2*) like that associated with the K-T impact (*3*) in the well-studied and documented Middle Devonian Eifelian-Givetian (E-G) (*4–6*) global boundary stratotype [GSSP (*7*)]. The magnetic susceptibility and biostratigraphic pattern reported here is seen in all other E-G sections that we and others have measured (*5, 6*) and is clearly global in extent. The impact interval occurs at the point in the E-G boundary section where magnetic susceptibility values begin a period of rapid oscillations. These oscillations start with low magnetic susceptibility values, representing a time of sea-level transgression, then rapidly rise immediately above the impact ejecta level. This rapid rise in magnetic susceptibility associated with the impact is very similar to what we observe for the K-T boundary interval, where we have interpreted the magnetic susceptibility oscillations as resulting from sea-level change and impact-induced erosional effects (*3*).

We examined samples collected from 11 m of section straddling the E-G GSSP boundary interval (*4*) and from a biostratigraphically well-studied and equivalent section at Bou Tchrafine, located 25 km to the northeast of Jebel Mech Irdane (*8*). The boundary intervals in these sections consist of thin, pelagic interbedded shales-marls and nodular limestones. Evidence for an impact ejecta layer is found at the same biostratigraphic level within the GSSP and at Bou Tchrafine and lies at the base of a shale-marl [bed 117 (*4*)] ~0.34 m below the biostratigraphic boundary that represents the base of the Givetian Stage. At the point where the ejecta evidence is first found, magnetic susceptibility values are low but then rise sharply (Fig. 1A), as predicted by extrapolation from our previous K-T results (*3*). The biostratigraphic boundary is defined by the first occurrence of the conodont species, *Polyg-nathus hemiansatus*, which evolved from a rapidly evolving conodont lineage that survived the Kacák/*otomari* global extinction event (*4*).

Carbon isotope ratios [δ13C (*2*)] were measured for 36 samples from the 11 m interval of limestones straddling the E-G stratotype. δ13C values for whole-rock carbonates range from –6.5 to +2.4 per mil (‰) PDB (the Pee Dee fossil belemnite standard) and define relatively uniform intervals punctuated by two negative δ13C spikes (Fig. 1A). Below –0.6 m, δ13C values vary narrowly about a mean of +0.7 ± 0.2‰ PDB ($n = 5$). The first δ13C spike begins with a shift of –9‰ to –6.5‰ at –0.37 m in the lower portion of the 0.25 m shale-marl at the Kacák/*otomari* extinction level (Fig. 1A). The δ13C values have recovered back to –0.5 ± 0.3‰ ($n = 3$) by –0.27 m. From –0.12 to –0.02 m and above 0.18 m, the δ13C values are markedly higher with +2.0 ± 0.6‰ ($n = 20$). These values are consistent with δ13C values measured in E-G marine calcite in nearby basins (*9, 10*), suggesting that E-G stratotype samples generally retain typical marine calcite values. The second δ13C spike represents a total negative shift of ~4‰ at 0.0 m, right at the beginning of the Givetian Stage (biostratigraphic level in Fig. 1A).

In the 11 m of the E-G GSSP measured for this study, the interval between –0.4 and –0.12 m shows enrichment in Ni, Cr, As, V, and Co (*2*) (Fig. 1B; table S1). Such high concentrations of these elements have been shown to be associated with impacts, either derived from the impactor or the target lithologies (*3, 11*). The bed in which the impact evidence is found is a gray shale-marl ~0.25 m thick, but in the lower portion of the bed, at the point where the geochemical anomalies begin, it has a slightly reddened color and very low magnetic susceptibility. The K-T boundary GSSP in Tunisia (*12*) is also located in a reddened layer near the base of a thin mudstone bed. In the E-G stratotype there is a second level, at ~0.0 m, with a negative δ13C shift of ~4‰. At this level, As is high, but Ni, Cr, V and Co are not. In addition, no shocked quartz or microspherules were found at this level.

We optically examined splits of samples throughout the E-G GSSP and at Bou Tchrafine, and we found 52 quartz grains

[1]Department of Geology and Geophysics, Louisiana State University, E235 Howe-Russell Geoscience Complex, Baton Rouge, LA 70803, USA. [2]Département de Géologie, Institut Scientifique, B.P. 703 – Rabat-Agdal, Morocco. [3]Department of Geology, University of Texas at Arlington, Post Office Box 19049, Arlington, TX 76019, USA.

Science

Interference of Quantized Transition-State Pathways in the H + D$_2$ $\rightarrow$ D + HD Chemical Reaction

Dongxu Dai, Chia C. Wang, Steven A. Harich, Xiuyan Wang, Xueming Yang, Sheng Der Chao and Rex T. Skodje

ARTICLE TOOLS	http://science.sciencemag.org/content/300/5626/1730
REFERENCES	This article cites 27 articles, 1 of which you can access for free http://science.sciencemag.org/content/300/5626/1730#BIBL
PERMISSIONS	http://www.sciencemag.org/help/reprints-and-permissions

Use of this article is subject to the Terms of Service